Tailor-Made Synthesis of Cerium Oxide Nanoparticles for Improving the Skin Decontamination of Paraoxon

Eloise Thomas, Stephanie Briancon, Frédéric Chaput, Greta Camilla Magnano, Isabelle Trenque, Delphine Arquier, Cynthia Barratier, David Amans, Thierry Devers, Isabelle Pitault, et al.

Tailor-Made Synthesis of Cerium Oxide Nanoparticles for Improving the Skin Decontamination of Paraoxon

Eloise Thomas[a*], Stéphanie Briançon[a,], Frédéric Chaput[b] Greta Camilla Magnano[a], Isabelle Trenque[abc], Delphine Arquier[a], Cynthia Barratier[a], David Amans[c] Thierry Devers[d], Isabelle Pitault[a], Karine Masenelli-Varlot[e], Matthieu Bugnet[f], Marie-Alexandrine Bolzinger[a*]

[a] Universite Claude Bernard Lyon 1, CNRS UMR5007, LAGEPP, 43 boulevard du 11 novembre 1918, Bâtiment CPE, 69622, Villeurbanne Cedex, France. eloise.thomas@univ-lyon1.fr; marie.bolzinger@univ-lyon1.fr

[b] École Normale Supérieure de Lyon, Universite Claude Bernard Lyon 1, CNRS UMR 5182, Laboratoire de Chimie, 46 allée d'Italie, 69364, Lyon, France

[c] Universite Claude Bernard Lyon 1, CNRS UMR5306, ILM, Bâtiment A. Kastler, 10 rue Ada Byron, 69622, Villeurbanne Cedex, France.

[d] Université d'Orléans, CNRS UMR7374, IUT Chartres, ICMN, 1b rue de la Férollerie, CS 40059, 45071, Orléans Cedex, France

[e] INSA Lyon, Universite Claude Bernard Lyon 1, CNRS, MATEIS, UMR5510, 7 Avenue Jean Capelle, Bât. B. Pascal, 4° étage, 69621 Villeurbanne Cedex, France

[f] CNRS, INSA Lyon, Université Claude Bernard Lyon 1, MATEIS, UMR5510, 7 Avenue Jean Capelle, Bâtiment B. Pascal, 4° étage, 69621 Villeurbanne Cedex, France

* Corresponding authors

KEY WORDS

Cerium dioxide – Nanoparticle - Skin decontamination - Paraoxon – Organophosphorus

ABSTRACT

CeO_2 nanoparticles possess a catalytic activity for hydrolysis of organophosphates such as paraoxon and nerve agents used in chemical warfare. Intoxication with these highly toxic compounds can occur directly through inhalation or dermal contact and lead to rapid and severe consequences including death. It is therefore necessary to have effective means of skin decontamination and CeO_2 nanoparticles are promising. In this study a wide range of CeO_2 nanoparticles were synthesized and their efficiency against paraoxon degradation was evaluated. Nano-cubes (NC), nano-rods (NR), nano-octahedra (NO) and nano-polyhedra (NPO) were studied along with nanoparticles obtained after calcination (NC*, NR*, NO* and nano-truncated octahedra NTO*). Results show an influence of calcination, specific surface area and crystal facets with higher activity for {111} facets compared to {100} facets. pH also impacted POX degradation rates, with higher pH accelerating the degradation. *In vitro* tests using the Franz cell method demonstrated the skin decontamination efficacy of CeO_2 nanoparticles. NC* exhibited lower efficiency, possibly due to smaller surface area and limited {100} facet degradation. The most efficient nanoparticles were NR* and NO* followed by NTO* consistently with their degradation efficiency and specific surface area. Notably, NR* and NO* performed comparably to FE (Fuller's earth), the standard powder skin decontaminant on battlefield. Unlike FE that can only adsorb paraoxon, CeO_2 nanoparticles can neutralize it into safer byproducts. This study highlights the interest of CeO_2 nanoparticles and the influence of their physico-chemical properties on organophosphorus compound degradation and cutaneous decontamination.

INTRODUCTION

Cerium, classified as a lanthanide element, exhibits thermodynamic instability in its metallic state when exposed to oxygen. As a result, cerium undergoes rapid oxidation, with the most stable form being CeO_2, also known as ceria. CeO_2 typically adopts a fluorite-type crystal structure[1] (space group $Fm\bar{3}m$). This structure consists of a face-centered cubic arrangement of Ce^{4+} cations, with all the tetrahedral sites occupied by O^{2-} anions. However, CeO_2 nanoparticles often display defects arising from the co-existence of Ce^{3+} and Ce^{4+} ions. CeO_2 is widely used in various applications, such as solid oxide fuel cells, catalysis, photocatalysis, gas sensors, fuel additives, UV protection etc.[1] In addition, nanoceria has attracted considerable attention in the biomedical field due to its protective effects against cellular damage caused by toxicants, radiation and pathological conditions.[2]

Recently, researchers have conducted thorough investigations into the catalytic properties of nanoceria concerning the hydrolysis of diverse organophosphates. These include pesticides, plasticizers and biologically active compounds. It was found that CeO_2 nanoparticles (NPs) demonstrated phosphatase mimetic activities, by catalyzing the cleavage of ester bonds in organophosphates and energy-rich biomolecules such as adenosine triphosphate (ATP).[3,4] Among organophosphorus (OPs) compounds, some can be used as pesticides or chemical warfare agents. These compounds are highly toxic, presenting significant hazards to both human health and the environment.[5] Numerous historical incidents serve as reminders of the devastating impact of these agents. Notable examples include the Tokyo subway sarin attack in 1995, the assassination of Kim Jong-Nam using VX nerve agent in 2017, the Salisbury poisoning incident involving the nerve agent Novichok in 2018 and the use of toxicants reported several times during the Syrian conflict. Organophosphorus nerve agents and pesticides can penetrate the body via the percutaneous pathway[6,7] leading to the inhibition of the

acetylcholinesterase enzyme. This inhibition results in accumulation of a neurotransmitter called acetylcholine and disturbs the normal process of neurotransmission. Severe skin contamination with highly toxic organophosphorus compounds can result in systemic toxicity, neurological effects, respiratory distress and death.[6,7] In order to limit the quantity of OPs in the bloodstream and prevent victims poisoning, a fast and rapid skin decontamination of OPs is therefore needed.

Various skin decontamination systems have been proposed, each differing on the materials used, their form (solid, liquid, etc.)[8] and their mechanism of action (adsorption or degradation of toxicants).[9] The simplest and most cost-effective strategy involves washing the skin with water or soap and water. However studies have revealed that these methods often result in incomplete decontamination[10] probably because of the oily nature and low solubility of the toxic substances in water. It may even lead to contaminant absorption due to the "wash-in" effect, promoting deeper penetration of toxins into the skin.[11] Fuller's earth has been frequently used as a decontaminant, acting as an effective adsorbent for various chemicals such as VX and mustard gas, reducing their penetration into the skin.[12–15] Fuller's earth can absorb the toxic substance but cannot destroy it. Several applications are needed to remove the toxic substance, which can be unwittingly inhaled once deposited on the powder and, which must be finally withdrawn. This process increases the risk of cross-contaminations even if a glove retaining the powder has been designed and could mitigate this risk.[12–15] Both methods (water wash or Fuller’s earth) do not completely degrade the toxicants, generating large quantities of toxic waste and increasing the risk of secondary contamination.[10,11] Decontamination systems able to degrade toxicants into safer by-products, like the Reactive Skin Decontamination Lotion (RSDL), offer a more advanced solution. As the liquid texture is difficult to handle, RSDL soaked in a sponge was developed to allow for better application. It rapidly and completely reacts with different chemical agents (G-agents, V-agents, etc.), producing relatively nontoxic

by-products.[12,16–20] However, this solution remains expensive. In the search for new efficient and cheap materials for skin decontamination, the ability of ceria nanoparticles (CeO_2 NPs) to degrade OPs into safer by-products appears highly interesting. We have previously successfully synthesized CeO_2 NPs and demonstrated *in vitro* their potential for the degradation of paraoxon (POX), a pesticide and model for OPs, in aqueous solution.[3,4,21–23] *In vitro* experiments, performed using the Franz cell method and skin explants, have also shown that CeO_2 as a powder or suspension is efficient to remove POX from the skin surface and to decrease skin absorption compared to the non-decontaminated control.[3,23] Other studies have focused on the use of ceria for the degradation of various chemicals as VX or Soman.[3,24–26]

While the potential of ceria for chemical degradation of toxic substances has been investigated, the impact of nanoparticles' physico-chemical properties on degradation remains insufficiently understood. Various factors such as the size, the shape, and the particle surface characteristics could have an impact.[1,21,22,27–30] Recently, we demonstrated the influence of CeO_2 NPs size, morphology and crystal facets on the degradation of paraoxon.[21,22] Zhan *et al.* have also studied the influence of morphology on model organophosphorus compounds and pointed out that the high catalytic performance of CeO_2 nanoparticles could be correlated with their exposed {111} and {110} facets, abundant oxygen vacancy sites, or specific Ce^{3+}/Ce^{4+} ratio.[29] Our study aims at completing these results by synthesizing diverse ceria nanoparticles to confirm the effect of morphology and calcination on POX degradation. Besides, some authors have pointed out the effect of pH on degradation of toxicants by a suspension containing metal oxide nanoparticles but contradictory results were obtained.[26,29,31,32] Therefore, the degradation kinetics of POX in a suspension of CeO_2 NPs at different pH values have been evaluated in this study.

Additionally, the assessment of metal oxide on skin decontamination and the study of the relationship between their structure and their efficiency were limited in previous research even if this is crucial to design an efficient decontaminant system based on CeO_2 NPs. In this article,

the *in vitro* efficacy of the developed CeO_2 nanoparticles as powder for skin decontamination is investigated using the Franz cell method, comparatively to Fuller's earth - the standard powder decontamination system.

RESULTS

With this interdisciplinary research we aim to underscore the significance of CeO_2 nanoparticles and their physico-chemical properties in the degradation and cutaneous decontamination of a model organophosphorus compound. By addressing the relationship between structure and function it could give valuable insights into the design of metal oxide for toxic compound neutralization and skin decontamination

NANOPARTICLES SYNTHESIS AND CHARACTERIZATIONS

Nanoparticles with different properties were prepared via a solvothermal process (**Figure 1**). Nano-cubes (NC), nano-rods (NR), nano-octahedra (NO) and nano-polyhedra (NPO) were obtained. At the end of the hydrothermal process, an annealing step was performed. After Calcination, NPs are labelled NC*, NR*, NO* and NTO* (nano-truncated octahedra resulting from NPO calcination). Morphological studies (TEM and BET analysis) and structural studies (XRD, XPS and Raman analysis) were carried out for all NPs (**Figure 2**, **Table 1** and SI). The diverse nanoparticles explored in this study build upon our prior research.[21,22] Our aim is to confirm and delve deeper into understanding the impact of the morphology, as well as the influence of calcination step on the degradation properties of nanoparticles.

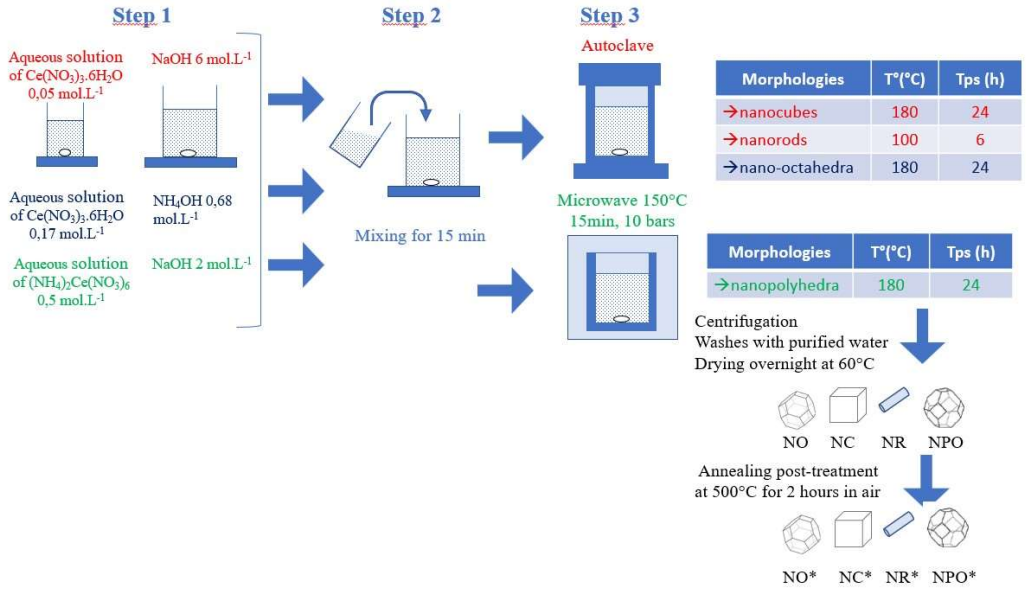

Figure 1: Synthesis of cerium oxide nanoparticles

***Table 1**: CeO_2 nanoparticles characterizations. NC, NR, NO and NPO represent nano-cubes, nano-rods, nano-octahedra and nano-polyhedra respectively. NC*, NR*, NO* and NTO* represent particles obtained after an annealing step at 500°C for 2 h).*

Sample name	Crystal facets	d_{MET} (nm)	S_{BET} ($m^2.g^{-1}$)	V_{pores} ($cm^3.g^{-1}$)	Mean pore diameter (nm)
NC	{100}	5-60	15	0.21	56.6
NC*	{100}	5-70	14	0.17	50.3
NR	Various crystal facets, including {111}	(7-9) x (50-200)	132.5	0.41	12,5
NR*	Various crystal facets, including {111}	(7-9) x (50-200)	90	0.67	31,7
NO	{111}	6-35	66.6	0,19	11,6
NO*	{111}	6-37	60.3	0,17	11,3
NPO	Not defined, including some {111}	~3	31.9	0,07	8,6
NTO*	{100}, {111}	~7	7.2	0,02	10,8

NC are polydispersed ranging in size from 5 to 60 nm, but all have an almost perfect cubic shape and are dominated by {100} facets. The size of NO ranges between 6 nm and 35 nm. NO are in an octahedron shape with truncation at the apexes and their surfaces are dominated by {111} crystal facets. For both NC and NO, diffraction patterns present only reflections

characteristic of the cubic fluorite structure of cerium dioxide. The lattice parameter of the NPs (5.4133 Å for NC and 5.416 Å for NO) are quite close to the value of the lattice parameter of bulk CeO_2 (5.411 Å). No significant modification of the morphology (size, shape, crystal facets,…) was observed with the annealing treatment (NC*, NO*) as shown on **Figure 2**, **Table 1** and Supplementary Information (**SI**).

NPO are in the form of nanoparticle agglomerates with a shape, which is not clearly defined. All the inter-reticular distances and angles between the crystallographic planes fit those reported in the ICDD file 00-034-0394 corresponding to cubic cerium dioxide (space-group 225, Fm-3m). Crystal facets are not well defined even if some {111} are observed. NR consist of rods about 7–9 nm in diameter and 50–200 nm long, which grew along the <110> direction. NR are porous, polycrystalline and present various exposed crystal facets, including {111} crystal facets. The lattice parameters for both NPO and NR are higher than previously reported (5.431 Å and 5.436 Å respectively). This can be attributed to the strain induced by twist boundaries or to the presence of Frenkel-type oxygen defects, where an oxygen atom is displaced from its lattice position to an interstitial site. Raman data are consistent with this conclusion. Raman spectra are dominated by a strong peak at 460 cm^{-1} (labelled F_{2g}, typical for the CeO_2 fluorite phase) and a weak band at 600 cm^{-1} (labelled D, assigned to oxygen defects, and most probably due to the presence of Frenkel-type oxygen defects)..

The intensity ratio I_D/I_{F2g} gives information about the fraction of intrinsic defect sites in the NPs. Values for NPO and NR (4.72 and 4.11 respectively) are 4 to 7 times higher than the values of the other particles indicating that NPO and NR have the largest fraction of Frenkel-type oxygen defects. However, XPS measurements show that the Ce^{3+}/Ce^{4+} ratio is less than 1% for NPO/NTO* and NR/NR* (**SI**) and support that the defects are more reliably attributed to the strain induced by twist boundaries. Contrary to the nanocubes and nano-octahedra, annealing induces several modifications to NPO and NR. For NPO, particles obtained after

annealing treatment are truncated nano-octahedra (NTO*). They are larger (the size is around 8 nm, compared with 3 nm before) and the facets are better defined and include {111} facets. The specific area of NTO* particles is also lower than that before annealing, due to particle growth by sintering during the annealing step. Sintering is also responsible for the decrease of the ceria surface area due to aggregation of particles during this step. In the case of nanorods, the annealing treatment did not affect the size nor the shape, but a decrease of the specific surface area was noticed. For both NPO/NTO* and NR/NR*, a decrease of the lattice parameter towards the bulk value (from 5.436 to 5.411 Å and from 5.431 to 5.413 Å respectively) and a decrease of the ratio I_D/I_{F2g} (from 4.72 to 0.67 and from 4.11 to 1.11 respectively) are noticed. Finally, the results show that the strain is considerably reduced and, this is consistent with an annealing in presence of oxygen in air, which is expected to induce a decrease of oxygen defects.[21]

The nature of the adsorbed species at the surface of the CeO_2 nanoparticles was characterized by infrared spectroscopy. All samples present adsorbed water and -OH groups at the surface as well as carbonate species formed by the adsorption of CO_2 from air. No significant differences were detected before and after the annealing step (data not shown).

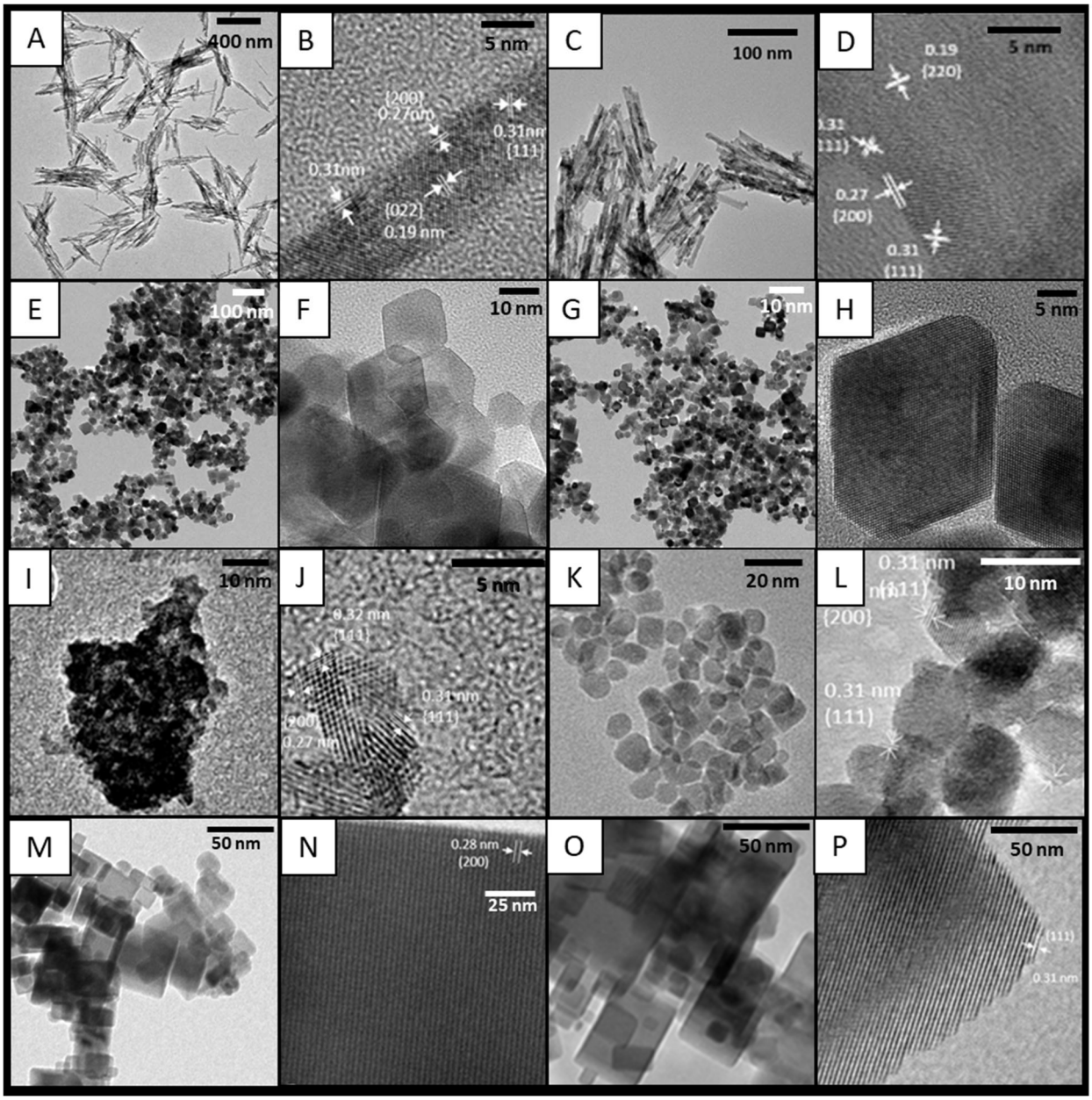

Figure 2: ***TEM and HRTEM images*** *of untreated and heat-treated cerium oxide nanoparticles* ***(A&B)*** *NR.* ***(C&D)*** *NR*.* ***(E&F)*** *NO.* ***(G&H)*** *NO*.* ***(I&J)*** *NPO.* ***(K&L)*** *NTO*.* ***(M&N)*** *NC.* ***(O&P)*** *NC*.*

IN VITRO DEGRADATION OF POX WITH NPS

Modelling

In order to understand which parameters impact the degradation of POX with CeO_2 NPs in an aqueous environment, Salerno *et al.* have previously modelled the degradation of POX *in vitro* and highlighted the importance of particles aggregation due to salts such as those in the

phosphate buffer at pH=7.4.[4] In the present study, in absence of salts, no aggregation is expected and a first-order kinetic model has been used to fit the data.

$$q_t = q_0 e^{-k} + q_\infty \quad (1)$$

with respectively q_0, q_t, q_∞ the percentage between the mass fraction of POX at t=0, at t and at infinity, versus the mass fraction of POX deposited in water. k is the degradation rate constant in min^{-1}. The reaction is fast or low but, in any case, tends towards zero and therefore, $q_\infty = 0$. Equation 1 has therefore been simplified and was written as follows:

$$q_t = 100 e^{-kt} \quad (2)$$

The curve fitting of the experimental values to the model allowed the determination of the rate constant (min^{-1}).

Influence of the morphology and calcination step on the POX degradation kinetics

The effect of CeO_2 NPs on POX degradation is illustrated on **Figure 3** and **Table 2**. No significant degradation of POX is detected without NPs, whereas the contrary is observed when NPs are added. Degradation kinetics depend on the type of NPs used as already observed elsewhere.[21,22] Taking into consideration morphologies that have never been studied before, degradation kinetic constants are ordered as follows: NC, NC* < < NPO < NTO* < NR << NR*, NO, NO*. For NPs for which the annealing step had no effect on their properties (NC/NC* and NO/NO*), there was no significant difference on POX degradation. Conversely, the reduction in defects and improved facet definition by the annealing step for NR/NR* and NPO/NTO* led to accelerated kinetics. The efficacy of POX degradation by NPs and the differences between NPs cannot be only explained by differences in specific surface area or pore volume. For instance, NTO*, which have the smallest values, lead to intermediate degradation kinetics. As described by Trenque *et al.*, the rate constant normalized by the specific surface area k/S_{BET} is more suitable to identify the most active facets.[22] The k/S_{BET} ratios follow the order: NPO < NC < NC* < NR < NR* < NO, NTO*, NO*. Thus, NPs with

ill-defined or {100} facets show low activity (NPO, NC, NC*), whereas particles with {111} facets exhibit higher efficiencies. These results confirm those obtained by Trenque *et al.*[22] However, the degradation rate of POX is better achieved using NR* compared to NTO* particles, each possessing {111} facets. This discrepancy can be attributed to NR* larger specific surface area. Zhan *et al.*[29] have also evaluated the effect of different morphologies of non-calcinated CeO_2 NPs on model OPs degradation. They observed a lower efficiency of nanospheres and nanocubes presenting {100} facets compared to nanorods ({110} facets) or nanopolyhedra ({111} and {100} facets). Our results are similar (NC/NC* and NPO are less efficient than NO/NO* and NTO*) and confirm the lower efficiency of {100} facets. However, they found that nanopolyhedra were more efficient than nanorods and this result departs from our own observations. This could be due to the fact that their NPs were not calcinated and, also to the fact that the NPO used in our study present a smaller size (3 nm against 13 nm for Zhan *et al.*), a smaller specific surface area (31.9 against 59.6 $m^2.g^{-1}$), a low pore volume (0.07 against 0.398 $cm^3.g^{-1}$) and, finally a higher mean volume diameter (8.6 against 22.8 nm).

Taken all together, our results indicate that the focus of future efforts should be directed towards synthesizing NPs that exhibit both high specific surface areas and {111} facets as this combination seems to enhance POX degradation efficiency.

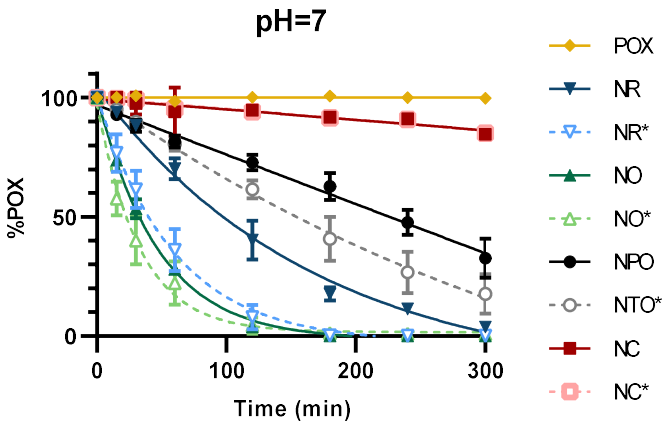

***Figure 3**: **Degradation kinetics of POX depending on NPs morphology and calcination step.** Representation of the mean ± SD.*

***Table 2**: **Kinetic constants of POX degradation** at pH=7 depending on NPs morphology and calcination step. k/S_{BET} and k/V_{pores} represent the normalized kinetic constants by the specific area and the pore volume, respectively.*

Sample name	R^2	k (min^{-1})	k/S_{BET} ($min^{-1}.m^2.g^{-1}$)	k/V_{pores} ($min^{-1}.cm^{-3}.g^1$)
NR	0.986	$5.94\ 10^{-3}$	$4.49\ 10^{-5}$	$1.45\ 10^{-2}$
NR*	0.997	$1.69\ 10^{-2}$	$1.88\ 10^{-4}$	$2.52\ 10^{-2}$
NO	0.997	$2.11\ 10^{-2}$	$3.16\ 10^{-4}$	$1.11\ 10^{-1}$
NO*	0.972	$3.03\ 10^{-2}$	$5.03\ 10^{-4}$	$1.78\ 10^{-1}$
NPO	*0.963* ¥	*~9.23 10^{-6}* ¥	*~2.89 10^{-7}* ¥	*~1.32 10^{-4}* ¥
NTO*	0.970	$2.36\ 10^{-3}$	$3.27\ 10^{-4}$	$1.18\ 10^{-1}$
NC	*0.597* ¥	*~2.31 10^{-5}* ¥	*~1.54 10^{-6}* ¥	*~1.10 10^{-4}* ¥
NC*	*0.868* ¥	*~6.26 10^{-5}* ¥	*~4.47 10^{-6}* ¥	*~3.68 10^{-4}* ¥

¥ *Ambiguous one phase decay model over the 5 h experiment.*

Influence of the pH on the POX degradation kinetics

The increase of pH enhances the degradation kinetics rate of POX in presence or absence of NPs, as shown on **Figure 4**, **Table 3** and **SI**.

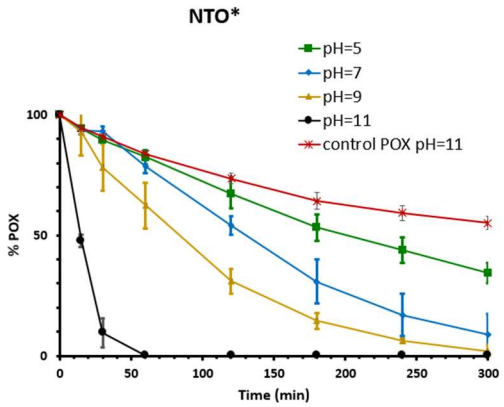

***Figure 4*: Degradation kinetics of POX depending on the pH for NTO*.** *Representation of the mean ± SD.*

***Table 3*: Kinetic constants of POX degradation depending on NPs morphology and pH.** *k/S_{BET} represents the normalized kinetic constant by the specific area.*

Sample name	pH	R^2	k (min^{-1})	k/S_{BET} ($min^{-1}.m^2.g^{-1}$)
NR*	5	0.9797	$1.246\ 10^{-2}$	$1.384\ 10^{-4}$
	7	0.9842	$1.691\ 10^{-2}$	$1.879\ 10^{-4}$
	9	0.9820	$4.121\ 10^{-2}$	$4.579\ 10^{-4}$
	11	0.9865	$1.773\ 10^{-1}$	$1.970\ 10^{-3}$
NO*	5	0.9727	$1.462\ 10^{-2}$	$2.425\ 10^{-4}$
	7	0.9720	$3.033\ 10^{-2}$	$5.030\ 10^{-4}$
	9	0.9669	$6.235\ 10^{-2}$	$1.034\ 10^{-3}$
	11	1.000	$4.086\ 10^{-1}$	$6.776\ 10^{-3}$
NTO*	5	0.9802	$2.782\ 10^{-3}$	$3.864\ 10^{-4}$
	7	0.9698	$2.356\ 10^{-3}$	$3.272\ 10^{-4}$
	9	0.9780	$8.108\ 10^{-3}$	$1.126\ 10^{-3}$
	11	0.9862	$5.887\ 10^{-2}$	$8.176\ 10^{-3}$
NC*	5	*~0.8291* ¥	*~1.746 10^{-5}* ¥	*~1.257 10^{-6}* ¥
	7	*~0.8680* ¥	*~6.255 10^{-5}* ¥	*~4.468 10^{-6}* ¥
	9	0.9562	$4.848\ 10^{-3}$	$3.463\ 10^{-4}$
	11	0.9636	$7.330\ 10^{-3}$	$5.236\ 10^{-4}$

¥ *Ambiguous one phase decay model over the 5 h experiment.*

For all NPs, the degradation of POX is faster when the pH increases. The kinetic constants are 15 to 30 times higher between pH 5 and 11 for NR*, NO* and NTO*. Few differences are visible for NC* compared to POX without NPs, maybe due to a slow degradation kinetics.

However, a significant synergistic effect is detected when {111} planes are combined with pH for NO*, NR*, and NTO*.

SKIN DECONTAMINATION

Skin decontamination efficiency was evaluated using the Franz cell method and pig-ear skin explants (**Figure 5**)**.** Paraoxon was chosen as it shares physicochemical properties and chemical functions with VX. It is a lipophilic substance, which therefore tends to be stored in the upper layers of the skin. It has been used as a simulant of V agents[33] because of its molecular weight and logP close to those of VX (275.2 $g.mol^{-1}$ against 267.4 $g.mol^{-1}$ and logP = 1.8 against 2.09 respectively for POX an VX). However, from a biopharmaceutical point of view, its skin penetration kinetics on pig skin is 4 times slower compared to VX on human skin. The POX applied dose was 13 $mg.cm^{-2}$ (or 10 $\mu L.cm^{-2}$) and corresponds to a full coverage of the skin. This is the dose recommended in the AFNOR NF X 52 122 for severe skin contamination. A late decontamination time was chosen (45 min after contamination of the skin) in order to allow time for POX permeation and to mimic a late decontamination procedure as it could be observed on battlefield. The decontamination process was carried out using water or powdered systems (Fuller's earth or CeO_2 nanoparticles). During decontamination, massage was avoided because massage or friction could push the toxic even deeper into the hair follicles.[34] After decontamination, the POX permeation study was continued over 24 h in order (i) to determine the impact of the decontamination process; (ii) to allow remaining POX to diffuse into the different skin compartments; (iii) to detect differences between the different decontamination systems.

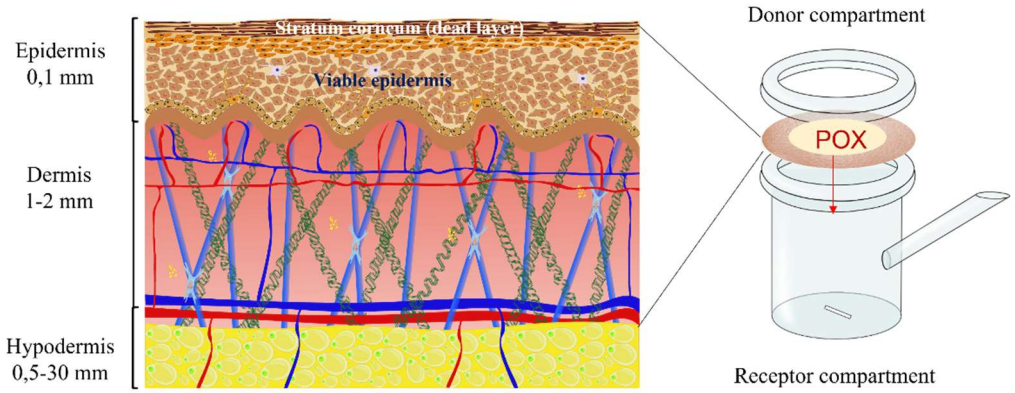

Figure 5: Structure of the skin and deposition of POX in a Franz diffusion cell

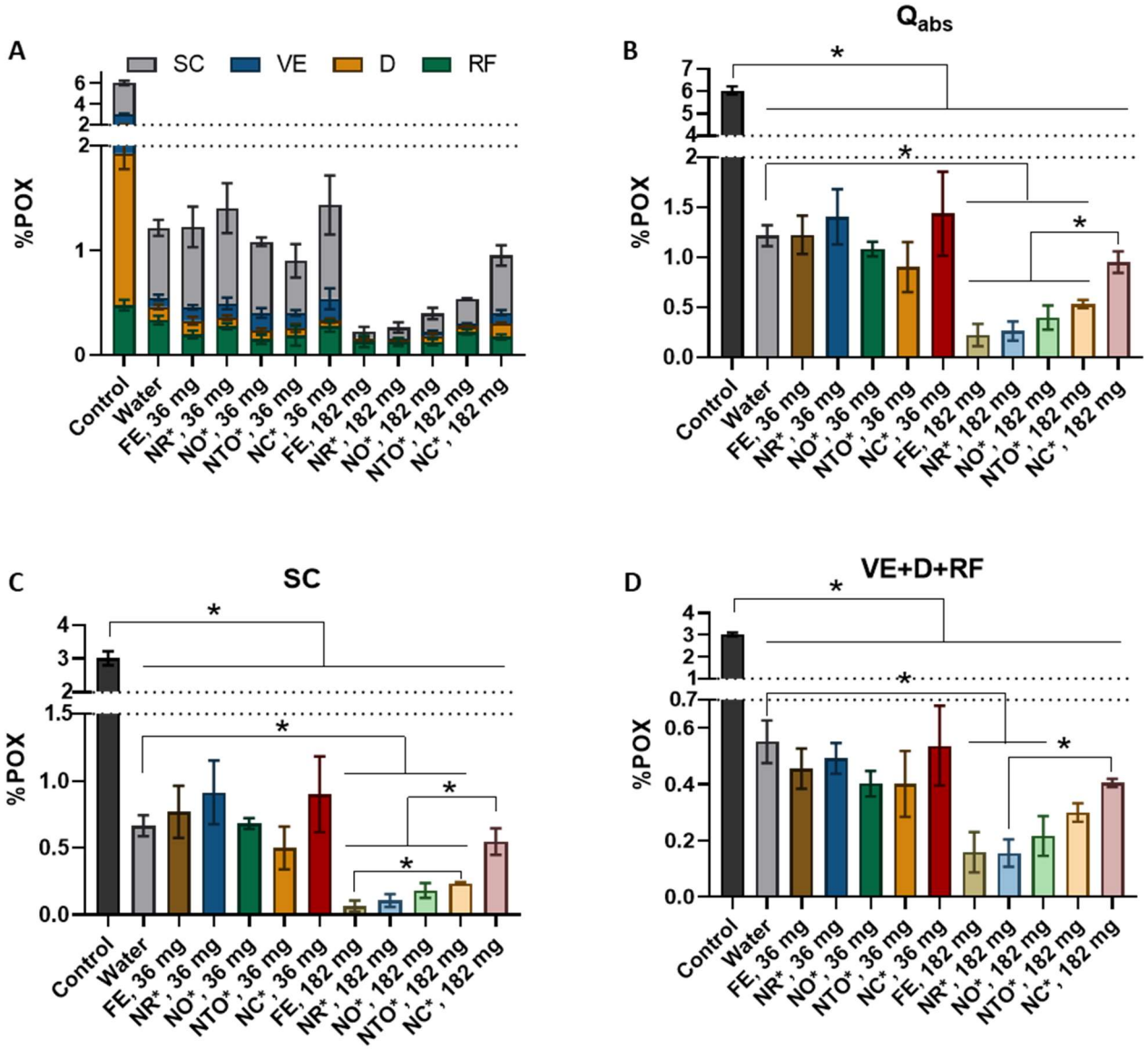

Figure 6:* Skin decontamination efficiency of the CeO_2 nanoparticles powder.** ***(A) *Percentage of POX at 24 h in the stratum corneum (SC), in the viable epidermis (VE), in the dermis (D) and in the receptor fluid (RF).* ***(B)*** *Percentage of POX at 24 h*

absorbed into the skin (SC+VE+D+RF). ***(C)*** *Percentage of POX at 24 h in the stratum corneum.* ***(D)*** *Percentage of POX at 24h in the viable skin (VE+D+RF). Results are expressed as mean ± SEM.*

Table 4*: In vitro distribution of POX through pig-ear full thickness unclipped skin 24 h after an exposure to POX with a decontamination at 45 min with Fuller's earth (FE) or CeO_2 nanoparticles. Results are expressed as % of POX applied dose (means ± SEM). F1 represents the reduction of the fraction of POX absorbed into the skin (SC+VE+D+RF) in comparison to control. F2 represents the reduction of the fraction of POX in the viable skin (VE+D+RF) in comparison to control ($F = \%_{control} / \%_{sample}$).*

	SC %	VE %	D %	RF %	F1	F2
Control	3.016 ± 0.209	1.089 ± 0.078	1.453 ± 0.151	0.477 ± 0.052	-	-
Water	0.666 ± 0.077	0.091 ± 0.028	0.126 ± 0.022	0.334 ± 0.041	4.96	5.48
FE, 36 mg	0.770 ± 0.194	0.129 ± 0.023	0.131 ± 0.038	0.196 ± 0.037	4.92	6.62
NR*, 36mg	0.915 ± 0.239	0.135 ± 0.055	0.083 ± 0.023	0.275 ± 0.031	4.29	6.13
NO*, 36 mg	0.683 ± 0.040	0.170 ± 0.046	0.083 ± 0.020	0.150 ± 0.044	5.56	7.50
NTO*, 36 mg	0.500 ± 0.160	0.143 ± 0.027	0.073 ± 0.038	0.186 ± 0.097	6.69	7.52
NC*, 36 mg	0.900 ± 0.283	0.208 ± 0.100	0.055 ± 0.021	0.275 ± 0.054	4.20	5.62
FE, 182 mg	0.066 ± 0.041	0.008 ± 0.004	0.021 ± 0.011	0.130 ± 0.060	26.89	19.06
NR*, 182 mg	0.108 ± 0.048	0.009 ± 0.004	0.023 ± 0.009	0.124 ± 0.037	22.88	19.32
NO*, 182 mg	0.182 ± 0.054	0.035 ± 0.017	0.059 ± 0.026	0.123 ± 0.030	15.15	13.96
NTO*, 182 mg	0.235 ± 0.009	0.027 ± 0.005	0.053 ± 0.008	0.220 ± 0.025	11.28	10.06
NC*, 182 mg	0.548 ± 0.097	0.103 ± 0.024	0.129 ± 0.007	0.173 ± 0.025	6.33	7.45

Figure 6A gives a general overview of the distribution of POX in each skin layer (namely the stratum corneum (SC), the viable epidermis (VE), the dermis (D) and the receptor fluid (RF)). It illustrates the efficacy of decontamination systems. More details with statistically significant differences between powders are reported in **Figure 6B to 6D**. The absorbed fraction (i.e., sum of the quantities from the SC to RF) is the quantity of chemical that can potentially move into the blood and is represented on **Figure 6B**. In all cases, powders are more efficient than the control, which is not decontaminated ($p<0.05$) with a reduction of the POX amount recovered into the skin ranging between 4.2 and 27.0 depending on the decontamination strategy. No statistical difference was detected between the use of 36 mg of powders and the use of water.

This result is not surprising considering that 36 mg of CeO_2 powder did not allow a total coverage of the skin surface on the contrary to FE (**Figure 7**). This led to a poor decontamination efficacy. The complete coverage of the skin surface was achieved by using five times more powder amount (182 mg). In this case, significant results were obtained. A significant statistical reduction ($p<0.05$) was demonstrated for all the powders except for NC*. A significantly higher decontamination efficiency is observed for NO*, NR* and NTO* compared to NC*. However, no significant difference is observed between FE, NR*, NO* and NTO*. Concerning the amount of POX absorbed into the skin, the most effective decontamination strategies seem to be the use of 182 mg of FE, NR*, NO* or NTO* with a respective reduction of the total amount of POX recovered into the skin of 27, 23, 15 and 11 compared to the non-decontaminated control (ratio $F1 = \frac{\%POX\ for\ the\ control\ in\ (\mathrm{SC+VE+D+R\ })}{\%POX\ for\ the\ decontaminant\ system\ in\ (\mathrm{SC+VE+D+RF})}$).

Similar conclusions can be drawn for the SC and viable skin (VE+D+RF) as illustrated on **Figure 6C and 6D**. For SC, that could act as a reservoir of toxic compound, the percentage of POX is always lower when a decontamination procedure is used comparatively to the control ($p<0.05$). Besides, the percentage of POX recovered into the SC is statistically lower when 182 mg of FE, NR*, NO* or NTO* are used in comparison to water ($p<0.05$). A significantly higher decontamination efficiency is observed for NR*, NO* and NTO* compared to NC* when a higher amount of powder is used (182 mg). However, again, no significant difference is observed between FE, NR* and NO*. For the viable skin (VE+D+RF), the percentage of POX is also always lower when a decontamination procedure is used than for the control not decontaminated ($p<0.05$). Trends are indicating that the percentage of POX is lower when 182 mg of powder are used in comparison to water, but statistically significant differences are only noticed for FE, NR* and NO*. Comparing CeO_2 nanoparticles, as previously, NC* appear

again to be the less efficient but the only statistical difference ($p<0.05$) is between NC* and NR*. No statistical difference is demonstrated between FE, NR*, NO* and NTO*.

Taken all together, the results disclose that the most efficient systems for skin decontamination are NR* or NO* powders applied as a full coverage onto the skin. Comparatively to FE, the advantage of both powders is their ability to degrade POX.

CeO_2 NANOPARTICLE SKIN PENETRATION

The penetration of CeO_2 nanoparticles into the skin was evaluated non-invasively using confocal Raman microspectroscopy (**Figure S2**). Indeed, ceria has a characteristic peak at 463 cm^{-1} that can be used to track the penetration of the particles into the skin. The peak of ceria was only observed on the top of the skin (Z = -2 µm). The ratios I_{463}/I_{1000} in the skin was on average of 0.5, showing that the peak of CeO_2 was twice less intense than that of the skin and blended with the background noise spectrum. These results indicate that the powder of CeO_2 NPs does not penetrate inside the skin.

DISCUSSION

An efficient skin decontamination technique should not only offer a fast and efficient removal of a toxic substance from the skin, but also its degradation to a compound having less or no toxicity.

OPs display different pathways of degradation, depending on their alkylation or arylation state and the nature of the nucleophile. Concerning POX, the nucleophilic attack can occur at the phosphorus center resulting in P–OAr cleavage ($SN_2(P)$), the aliphatic carbon with C–O cleavage (SN2(C)), and/or the aromatic group with Ar–O cleavage (SNAr). [35,36]Metal oxides

(TiO_2, MgO, ZnO, Al_2O_3…)[37–42] have emerged as promising nanomaterials to enhance the decontamination efficacy against organophosphorous compounds. These NPs possess unique properties, such as high surface area and chemical reactivity, allowing for effective binding and neutralization of toxic agents. These nanoparticles are also less expensive than other decontamination systems (~10€/g for CeO_2).[21] Amongst metal oxide NPs, CeO_2 has also been shown to absorb the OPs and degrades them to a less toxic element.[3,24–26,43] Several recent studies have demonstrated its efficacy against a simulant molecule of a chemical warfare agents of the G-series like sarin (GB) gas but also against HD.[37,44,45] Degradation of OPs as POX implies the cleavage of the P–O aryl bond. The attack at the phosphorus center, $S_N2(P)$, has been reported as the sole reaction pathway. The main degradation products are diethyl phosphate and p-nitrophenol. [3, 24–26, 43] In contrast to POX, PNP does not affect the cholinesterase activity. Paraoxon is very toxic, with an acute oral toxicity and a dermal acute toxicity LD50, respectively estimated to 0.5mg.kg^{-1} and 50mg.kg^{-1} in rats. The acute oral and dermal acute toxicities are significantly increased for p-nitrophenol (acute oral toxicity in rats LD_{50} estimated to 230mg.kg^{-1} in rats, dermal acute toxicity in rabbits LD50 >5000mg.kg^{-1}) compared to POX.[46, 47] ~~A nucleophilic substitution (SN_2) has been proposed to be the main mechanism responsible for this cleavage.~~ The mechanism can be divided in different steps as presented on **Figure 7**. First, the coordination between the phosphoryl oxygen and a Ce atom leads to the adsorption of the toxic. The phosphorous atom is therefore more susceptible to undergo a nucleophilic attack. In a second step, an hydroxyl group coordinated with a Ce atom near the adsorption site, acts as a nucleophile towards the P atom, and the subsequent SN_2 reaction leads to the cleavage of the P–O-aryl bond, and the release of p-nitrophenol.[1] As this reaction happens at the surface of the NPs, it is easily understood that specific area will play a crucial role in POX degradation efficiency. However, as demonstrated in this study, it cannot be the single factor impacting the degradation of POX. The number of hydroxyl groups appears

to be also important, as previously reported in different studies.[26,27,48] Delving deeper into the aforementioned mechanism can also provide an explanation for the observed influence of crystal facets on POX degradation, as highlighted by our study. The difference between facets reactivity can be explained first by the adsorption probability, assuming the coordination between the phosphoryl oxygen and Ce atoms. As the surface density of Ce atoms is higher for the {111} crystal facets, than for the {100} facets, the adsorption on {111} facets is favored. Besides, the surface density of the Ce–Ce with a distance of 0.383 nm (needed for the SN_2 of OH on POX adsorbed on a neighboring Ce atom) for {111} facets is almost twice the surface density for the {100} facets. Both criteria appear to favor the {111} facets and can explain their higher reactivity.[22] Studies on CO oxidation or acetaldehyde adsorption confirmed the difference in reactivity according to the crystal facets.[49,50] Subsequent studies have provided additional detailed insights into the mechanism of POX interaction with CeO_2 NPs.[5,27] The catalytic activity of CeO_2 NP relies to the existence of oxygen vacancies related to the reduction of Ce(IV) to Ce(III). It has been described that Ce(IV) would be more effective than Ce(III) to adsorb POX. On the other hand, hydroxyl groups bounding to Ce(III) would be favored on Ce(III) in comparison to Ce(IV).[5,27] Therefore the most effective active site for POX degradation would contain a hydroxyl group bound to the Ce(III) localized in the vicinity of Ce(IV): a certain spatial arrangement of several atoms and functionalities is required, similar to some extent to the role of enzymes in enzymatically catalyzed reactions. In a last step of the mechanism, the migration of oxygen vacancies supports the generation of Ce(III) followed by the creation of a new reactive site.[26] The ease of reduction of Ce(IV) to Ce(III) accompanied by the creation of oxygen vacancies highlights the interest of CeO_2 material. Ederer et al. have recently studied the influence of CeO_2 particles treated with various chemicals on the inorganic phosphate adsorption and catalytic decomposition of POX. Any direct relationship was noticed between the relative amount of oxygen vacancies and the catalytic activity. It seems that the

number of surface hydroxyl groups, surface area and crystallites size were more important for OPs degradation.[1,51] Moreover, simple and robust crystalline lattice of cerium oxide enables vacancy migration within the nanoceria matrix, rendering the active sites on its surface dynamic in nature.[27] This information can explain the influence of calcination that we and other teams observed. Calcination can improve crystallinity that may be favorable for degradation of POX. However, high calcination temperature also decreases surface area and the number of surface hydroxyl groups and could in turn lead to a decrease in POX degradation.[1,26,27,43] An annealing temperature of 500°C seems to be a good compromise to maximize the CeO_2 efficiency. To conclude, a complex set of physical and chemical characteristics (surface area, facets, number of surface hydroxyl groups, etc.) has to be considered to synthesis CeO_2 NPs with efficient degradation properties.

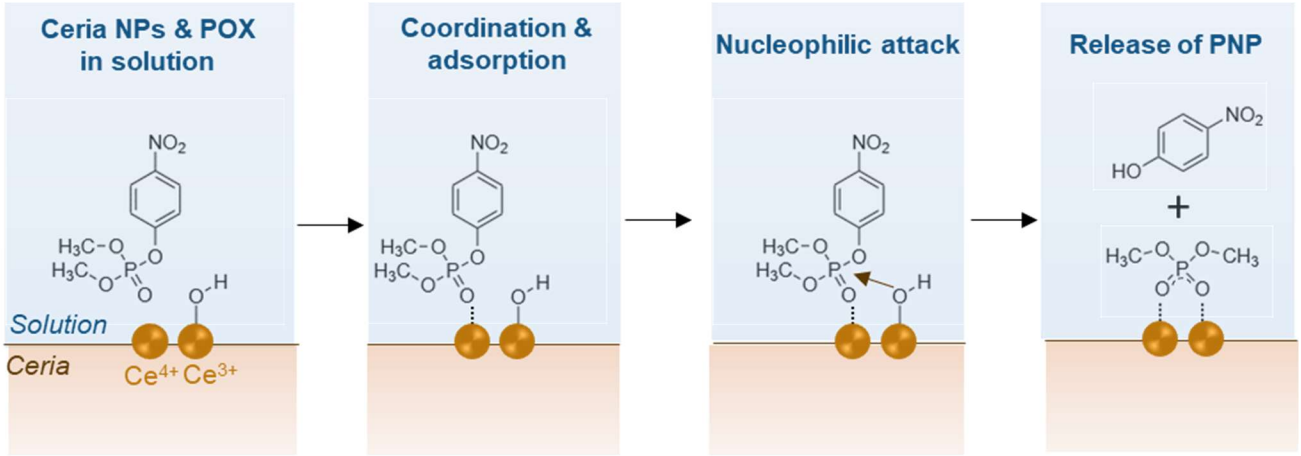

***Figure 7*: Degradation of POX to PNP by the CeO_2 surface.** Adsorption of paraoxon through the coordination between the phosphoryl oxygen and a cerium ion followed by an SN_2 reaction leading to the cleavage of the P–O-aryl bond, and formation of diethylphosphate and p-nitrophenol.

Other factors are affecting the degradation kinetics of OPs by CeO_2 NPs, as the pH of suspension, and contradictory results have been presented in the literature. Kuchma *et al.*[32] found that the activity of CeO_2 NPs was higher at lower pH with an initial relative rate of the reaction of 1.7, 1 and 0.1 for pH 4, 7 and 10 respectively. They explained that it could be due

to different reaction pathways or possibly to changes in the surface charge of the nanoparticles at basic pH. Our study showed the opposite with a higher degradation activity of NPs in alkaline conditions. These results are in agreement with the one of Janos *et al*.[26], Zhan *et al.*[29] , and Miri *et al*[31]. The higher efficiency may be related to the acid–base properties of 4-nitrophenol making it a better leaving group at higher pH[26] or to a change in the surface of CeO_2 NPs. Vincent *et al*[52] have explained that CeO_2 NPs in suspension can adsorb protons (H^+ ions) or OH^- ions. When the pH of the suspension is acidic, CeO_2 absorbs a proton and forms a positive charged particle. In this case, the H^+ ion is covalently bound to the CeO_2 surface oxygen. On the contrary, when the pH of the suspension is high, negatively charged colloid particles are obtained. In this case, the OH^- ion is ionically bound to the CeO_2 surface. Miri *et al.* have demonstrated that the OH^- ions adsorbed on the CeO_2 NPs surface are very strong nucleophiles that attack the phosphorous center of POX. The entity responsible of the degradation of POX is indeed the OH^- bound on the surface of the NP and not other nucleophiles as HO^- or H_2O present in solution.[31] Taken together, this information explains why at basic pH the degradation of POX is increased. To go further, Vincent *et al.* have performed DFT simulations for an octahedral NP derived from a bulk cerium oxide fluorite lattice, exposing the most stable {111} facets.[52] They demonstrated that there are two equilibrium positions for OH^- ions: one on the facet position, in-between the three oxygen atoms terminating the NP surface, and the other position in the vertex of the NP near the cerium ion. Among the two different equilibrium positions for OH^-, the vertex position is the more stable one. As adsorption of OH^- on CeO_2 NPs depends on the facets, it is likely that different results would be obtained for different morphologies. This could explain why no effect of the pH was detected in our studies for NC* particles presenting {100} crystal facets. Another explanation would be that as the degradation of POX with NC* is so slow, that no difference could be detected in the time course of the experiment concerning the pH. It is therefore very appealing to tune the pH of particles

suspensions, shape and crystallographic planes all together in order to obtain the highest POX degradation kinetic *in vitro* and once the particles are spread onto the skin.

In this study, we validated the efficacy of CeO_2 NPs for skin decontamination using Franz diffusion cells, and compared the results with water and FE, the standard decontamination system used as powder. As a first proof of concept, we studied here the use of CeO_2 NPs as powder as Salerno *et al.* found that aqueous dispersions of CeO_2 did not achieve good degradation efficacy compared to powder probably due to the presence of the buffer and an anionic gelling agent in the formulation.[3] In this previous work conducted by our team, we assessed the effectiveness of a skin delayed decontamination of POX using CeO_2 particles. The same amount of POX was deposited onto the skin. After 1h, 36mg of CeO_2 as a powder or an aqueous suspension were deposited for decontamination purposes. FE and RSDL® (Reactive Skin Decontamination Lotion) were used as controls for CeO_2 powder and CeO_2 suspension respectively. FE is an absorbing powder with a large specific area and selectivity for lipophilic molecules, which is not able to degrade the toxic. This is the reference decontamination powdered system used by the French Army. It was chosen as a control for comparing the efficacy of powders in both studies. RSDL is also a reference system often used to compare the efficacy of liquid decontamination systems. This medical device is a basic (pH~10) lotion designed to solve lipophilic molecules and neutralize toxic agents. The F1 ratios calculated here from this first study are respectively 3 for FE and 12 for RSDL. The F1 ratio for CeO_2 powder is only equal to 1 while it is equal to 9 for the CeO_2 suspension, despite its low degradation efficacy. The ratio for FE is not the same between both studies (3 against 4.9 in the present study) because of the delay before applying a decontaminant (1h against 45 min). This first study confirmed that it is necessary to tune the shape of the particles to achieve better degradation and then decontamination efficacies. As usual, RSDL displayed good decontamination properties but this medical device comprises a pouch impregnated with a

lotion sealed in a foil and is better dedicated to the treatment of small area. [3,11,53] Moreover, its storage stability is questioned if the recommended storage conditions (15°C-30°C) are not applied.[54] It seems therefore important to preserve bare CeO_2 particles themselves, and to tune their properties to achieve high degradation kinetic properties. It should also be noted that POX contains a part of water and that the skin is a wet organ that continuously loses water permeating freely from the dermis (TransEpidermal Water Loss flux, around 10 $\mu g.cm^{-2}h^{-1}$). The water present at the skin surface should therefore be sufficient to create the good condition for POX degradation. The use of 36 mg of CeO_2 powder did not yield statistically significant differences compared to water alone, probably due to an incomplete coverage of the skin surface. However, when the amount of powder was increased by a factor 5, from 36 to 182 mg, a complete coverage was achieved, resulting in an improved decontamination efficiency. At this level, except for NC*, all CeO_2 NPs allowed a reduction in POX absorption into the skin, indicating that the powders slow down POX penetration compared to a water wash. FE demonstrated a high effectiveness, attributed to its high specific surface area (120 to 140 $m^2.g^{-1}$) and, excellent adsorption capacity. Despite the lower specific areas of NR*, NO*, and NTO* (90, 60 and 7 $m^2.g^{-1}$ respectively), the three types of CeO_2 NPs exhibited similar efficiency to FE, likely due to their degradation ability, highlighting the potential of such systems for decontamination. The Figure 8 illustrates the POX degradation by CeO_2 particles on the skin. The Figure 8A shows the beginning of the decontamination step (36mg of NO*applied on 25.4µL of POX deposited on the skin 45min ago), while Figure 7B illustrates the end of the experiment with the same particles. The powder becomes yellow indicating the production of p-nitrophenol. The same experiment was performed in our research team using a peelable gel incorporating nanoceria.[23] The decontamination system became yellow in the presence of NO in the gel and PNP was detected as the main degradation product by HPLC after 30 min of contact. The same mechanism occurs after contact with the skin.

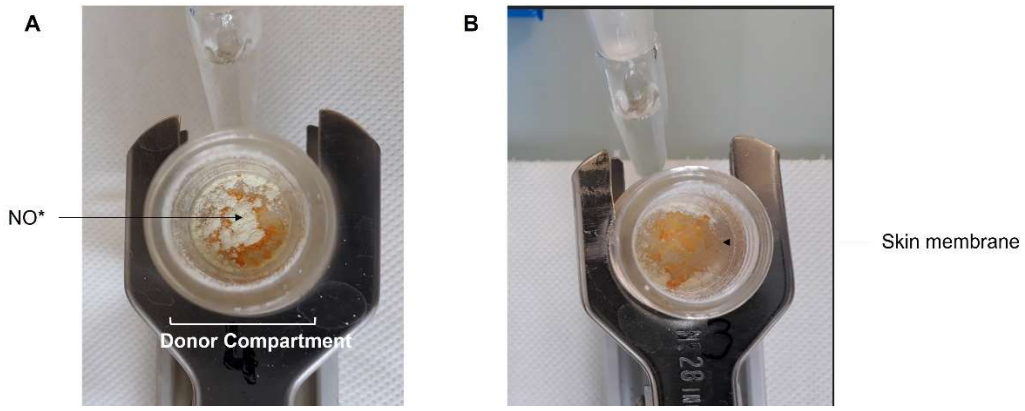

***Figure 8*: Degradation of POX to PNP by the CeO_2 surface on the skin.** POX was deposited in the donor chamber of the Franz cell onto the skin surface**.** After 45min NO* was added (36mg) in the donor chamber and the picture shows that this quantity is not enough to recover the full skin surface. After 24h the skin surface is yellow indicating the conversion of POX into p-nitrophenol.

NC* showed lower efficiency, possibly due to its smaller specific area (14 $m^2.g^{-1}$) and limited POX degradation ability as presented before. The analysis of POX recovery in the stratum corneum (SC) and viable skin (VE+D+RF) indicated that the most efficient CeO_2 NPs for skin decontamination were NR* and NO*, followed by NTO*. This result is consistent with their degradation efficiency and specific surface area. No significant decontamination efficacy was noticed between NR* and NO* in spite of a higher degradation kinetic constant value for NO* compared to NR*. This may be due to the absence of water in the decontamination system, which smooths the results. In our previous study the decontamination efficacy of CeO_2 water suspension, was higher than that of powder while the degradation efficacy of powder was superior compared to suspension.[3] Overall, NR* and NO* demonstrated similar efficiency to FE, the standard powder system, for skin decontamination. However, it is worth noting that CeO_2 NPs have the added advantage of neutralizing POX into safer byproducts as demonstrated in previous publications[3,4,21–23] which FE does not achieve. This emphasizes the potential benefits of utilizing such nanoparticle-based systems for effective skin decontamination.

The potential toxicity of ceria particles is an important consideration that may affect their widespread application. Forest *et al.* conducted an *in vitro* study on macrophages from the RAW264.7 cell line to investigate the effect of ceria nanoparticle morphology.[2] Results showed

no ROS production, whatever the nanoparticle shape but the LDH release and the TNF-α production were significantly and dose-dependently enhanced by rod-like nanoparticles, whereas they did not vary with cubic/octahedral nanoparticle.[2] Considering this crucial aspect, the preference for NO* nanoparticles emerges as a promising choice for decontamination purposes. Research concerning their formulation into easy-to-handle skin decontamination systems should be carefully examined.[23] Besides, we have shown that the CeO_2 NPs powder used in this study should not be able to penetrate the human skin under normal conditions. From a general point of view, penetration of NPs depends strongly on their size and on the integrity of the skin. NPs with a size below 4 nm can penetrate and permeate into intact skin. When the size is increasing, the permeation decreases. Therefore, NPs size between 4 and 20 nm can potentially permeate intact and damaged skin whereas NPs size between 21 and 45 nm can penetrate and permeate only damaged skin. Finally NPs size > 45 nm cannot penetrate nor permeate the skin.[55] In our study, the CeO_2 powder is composed of small particles but calcination induced aggregation of the NPs and their use as powder surely prevents penetration of ceria in the skin which emphasizes their interest for skin decontamination purpose. Another strategy to mitigate particle penetration into the skin could involve trapping the particles within a matrix applicable to the skin that effectively retains them. Recently, we have formulated an easy-to-handle peelable gel incorporating CeO_2 nanoparticles. The efficacy of this peelable gel has been prominently demonstrated, showcasing a remarkable 5-fold reduction in the quantity of POX absorbed into the skin and a substantial 3–4-fold decrease in viable skin in comparison to the non-decontaminated skin.[23]

CONCLUSION

Skin contamination with toxic agents remains a significant concern, prompting the ongoing search for effective decontamination systems. These systems should not only remove toxic substances from the skin but also degrade them to neutralize their harmful effects. Among the reactive sorbents being extensively investigated, metallic oxide nanoparticles (NPs) are of particular interest due to their unique adsorbing and destructive properties stemming from their morphology, crystal structure, porosity, and catalytic characteristics. In this context, CeO_2 nanoparticles have shown interesting promise. This study demonstrates that the efficacy of CeO_2 NPs for degrading toxic substances like POX and decontaminating the skin depends on various factors, such as shape, calcination, crystal facets, and specific surface area. The study highlights the potential of nano-octahedral CeO_2 (NO*), showing similar decontamination efficiency to FE (a reference material), but also the ability to degrade organophosphorus compounds into safer products. To fully capitalize on the degradation capabilities of CeO_2 NPs for toxic agents, it would be beneficial to formulate these nanoparticles into a skin-friendly product that can be easily applied and removed. A fine selection of the pH of the formulation could also increase the degradation of toxics as demonstrated with the degradation experiment in vitro. Actually, the skin is acidic with a pH of 5.5 and, we could take advantage of suspending CeO_2 in a basic medium (~9) to decontaminate the skin. This advancement would offer a practical and efficient means of combatting skin contamination by toxic substances.

EXPERIMENTAL SECTION

MATERIAL

POX (O,O-diethyl p-nitrophenyl phosphate, purity 90%) was purchased from Sigma Aldrich (Saint-Quentin-Fallavier, France). Cerium nitrate hexahydrate $Ce(NO_3)3 \cdot 6H_2O$ (99.5%, cerium oxidation state +III) and cerium ammonium nitrate $Ce(NH_4)_2 \cdot (NO_3)_6$, (99.5%, cerium oxidation state +IV) were purchased from Alfa Aesar (Kandel, Germany). The first cerium precursor was used for the manufacturing of nanorods and nanocubes, whereas the second was used for the manufacturing of nano-octahedra. Sodium hydroxide (98%), potassium hydroxide and ammonium hydroxide were bought from Carlo Erba, (Peypin, France). Fuller's earth was supplied by NBC-Sys (St Chamond, France). Ethanol (96.3%), methanol and glacial acetic acid (HPLC grade) were purchased from Fisher Scientific (Illkirch-Graffenstaden, France). Ultrapure water, (resistivity > 18 MΩ.cm) was used as receptor fluid of Franz cell and as degradation medium in vitro. All chemicals were purchased and used without further purification.

METHODS

Synthesis of CeO_2 NPs

The synthesis of nano-rods (NR, NR*), nano-octahedra (NO, NO*) and nano-cubes (NC, NC*) were performed via an hydrothermal process following the protocol of Trenque *et al*.[21,22]

Briefly, $Ce(NO_3)_3 \cdot 6H_2O$ was reacted with NaOH or NH_4OH and the mixture heated in an autoclave before being cooled down. The obtained fresh precipitate was washed with distilled water and recovered. By varying the experimental conditions (initial concentration of $Ce(NO_3)_3 \cdot 6H_2O$ or reaction temperature), different morphologies were obtained : NR, NO or

NC. In order to perfect the crystallinity of the nanoparticles, a heat treatment was carried out on all the nanoceria at 500°C in air for 2 hours. The obtained nanoparticles are named respectively NR*, NO* and NC* after calcination of NR, NO and NC.

The synthesis of nano-polyhedra (NPO) and nano-truncated-octahedra (NTO*) was performed following the protocol of Salerno *et al.*[3] Briefly, an aqueous solution of ammonium cerium (IV) nitrate at 0.5 mol.L^{-1} was mixed with an aqueous solution of sodium hydroxide (2 mol.L^{-1}). The precipitation was carried out in a microwave digestion system (Multiwave-3000, Anton Paar) at 150 °C for 15 min. After cooling to room temperature, the obtained nanoparticles (NPO - nanopolyhedra) were isolated by centrifugation, washed with distilled water and dried at room temperature overnight. NPO were then calcinated at 500°C for 2 h and nano-truncated octahedra (NTO*) were obtained (as presented in the Results section).

Characterizations of CeO_2 NPs

The particles were characterized as described by Trenque *et al.* [22] Briefly, they were observed by transmission electron microscopy (TEM) using a JEOL 2100 HT operating at 200kV. High-resolution transmission electron microscopy (HRTEM) images were also performed. The specific surface area was calculated from the adsorption/desorption isotherms of nitrogen at 77 K using a BELSORP-max instrument (Passy, France). The Brunauer–EmmettTeller (BET) method was used for surface area calculation. X-ray diffraction (XRD) patterns were recorded on a Bruker D8 Advance diffractometer equipped with a sealed Cu X-ray tube (40 kV, 40 mA) and a linear Lynxeye XE detector. The lattice parameters and the crystallite sizes were extracted from XRD patterns by profile matching (LeBail fit) using the elementary pseudo-Voigt function with the FullProf program packages. XPS measurements were performed on NR/NR*and NPO/NTO* powders to calculate the Ce^{3+}/Ce^{4+} ratio. XPS measurements were carried out using an AXIS Ultra DLD instrument from Kratos Analytical instrument using monochromatic Al Ka X-rays. The CeO_2 powders were embedded in an indium foil and mounted on a stainless-

steel sample holder. The Ce^{3+}/Ce^{4+} ratio was calculated by modelling the area of the experimental spectrum with a linear combination of the areas of two experimental spectra of Ce^{3+} and Ce^{4+}. Sample charging was minimized using a charge compensator system.

In vitro degradation of Paraoxon

The *in vitro* degradation of POX was performed (number of experiment repetitions: n=3-5). Suspensions of NPs in water were prepared and the pH adjusted to the desired value with an HCl or NaOH solution. The temperature of the suspension was then adjusted at 32°C. At t=0, a solution of POX was added to 2 mL of NPs suspension containing 200 mg of NPs to reach a POX concentration of 55 $\mu g.L^{-1}$. Suspensions were stirred at 32°C for 5 h. At different time points of contact between POX and NPs, supernatant was collected, diluted by 10 in water, filtrated on 0.2 µm to remove NPs and analyzed with HPLC. The GraphPad Prism 8.4.2 software was used to fit the data.

Quantification of POX by HPLC

POX was analyzed from samples using high-pressure liquid chromatography equipped with a XTerra® MS-C18 column (5 µm, 4.6 mm×250 mm) as already described [3,22]. An HPLC Waters Alliance 2695 coupled with a 2998 photodiode array detector (PDA), working at 269 nm, was used. The column oven temperature was maintained at 40°C. The calibration curve was prepared between 0 and 100 $\mu g.mL^{-1}$. The elution of 10 µL of the samples with methanol/water (acidified with 0.5% (v/v) acetic acid) at a flow rate of 0.7 $mL.min^{-1}$ gave a retention time of 7.5 min for POX. For all experiments, samples were filtrated on 0.45 µm membrane disc filter before injection.

Evaluation of skin decontamination efficiency

Pig-ears were collected immediately after animals were killed (Ecole de Chirurgie, University Lyon1, France). They were stored flat at -20°C for a maximum period of 6 months. The skin was prepared following the procedure described elsewhere.[56] Five replicates for each decontamination systems were performed. On the day of the experiment, the skin samples (1.2 ± 0.1 mm thick) were thawed and mounted on Franz-type static glass diffusion cells with a surface area of 2.54 cm². Ultrapure water was used as acceptor medium. The cells were maintained at 37°C in a water bath in order to reach the skin surface temperature of 32 ± 1°C. Skin integrity was assessed by measuring the transepidermal water loss. Following the OECD guidelines (OECD, Organisation for Economic Co-operation and Development, 2004), only skin with transepidermal water loss values ranging between 3 and 10.g.h^{-1}.m^{-1} were used in the skin penetration studies. The donor compartment remained open during the time of the experiment.

For the decontamination study, 25.4 µL of pure POX divided into microdroplets were applied of the pig-ear skin surface in the donor compartment of the cell. This resulted in an applied dose of Q_0 = 13 mg.cm^{-2} (or 10 µL.cm^{-2} or 46 µmol.cm^{-2}) and corresponded to a full coverage of the skin.

After 45 minutes of exposure to the toxic, the skin was decontaminated by applying the different decontamination systems. 36.4 mg or 182 mg of powder (FE or CeO_2 NPs) were deposited by sprinkling the entire surface with the powder. Two minutes after deposition, the powder was removed by washing 3 times with 3 mL of distilled water and dried with a tissue. As control, tests were performed following the same protocol but without addition of powder (samples are called water in the following). Finally, some skin samples were not decontaminated at all and are referred as “control” in the following.

24 h after POX exposure, the receptor fluid (RF) was collected and skin samples were removed from the diffusion cells. The first strip was quickly removed using D-Squame tape (Monaderm). This first strip represents the POX accumulated into the fine wrinkles of the skin after decontamination with the powder. The stratum corneum (SC) was separated from the viable epidermis (VE) and dermis (D) by strips and placed in vials each containing 3 mL of ethanol (12 strips were used during this step). Then, the viable epidermis was separated from the dermis and deposited in a vial containing 2 mL of ethanol. The vial was maintained for 2 h under magnetic stirring at room temperature to extract POX. The dermis was cut into small pieces and placed in a vial containing ethanol. It was extracted 4 times under magnetic stirring at room temperature, one time with 4 mL EtOH and 3 times with 2 mL EtOH. After each extraction, the aliquots were diluted if needed and filtered on a nylon membrane disc filter (45 µm pore-size, 25 mm diameter) before HPLC quantification. It was verified that this protocol leads to a recovery of POX above 85% for the control samples.

The mean standard error (SD) and standard error of the mean (SEM) were calculated (n = 4-5). Statistical comparisons were made using the Student's t-test after checking that the variance were not equal (Mann-Whitney test) with the level of significance at $p < 0.05$.

Two ratios were calculated to compare the different decontaminant systems with the control (no decontamination): F1, F2.

$$F1 = \frac{\%\ of\ POX\ for\ the\ control\ in\ (\mathrm{SC} + \mathrm{VE} + \mathrm{D} + \mathrm{RF})}{\%\ of\ POX\ for\ the\ decontaminant\ system\ in\ (\mathrm{SC} + \mathrm{VE} + \mathrm{D} + \mathrm{RF})}$$

$$F2 = \frac{\%\ of\ POX\ for\ the\ control\ in\ (\mathrm{VE} + \mathrm{D} + \mathrm{RF})}{\%\ of\ POX\ for\ the\ decontaminant\ system\ in\ (\mathrm{VE} + \mathrm{D} + \mathrm{RF})}$$

F1 corresponds to the ratio for the percentage of POX absorbed into the skin (SC+VE+D+RF), F2 corresponds to the ratio for the percentage of POX in the viable skin.

Evaluation of CeO_2 nanoparticles penetration into the skin

Confocal Raman microspectroscopy was used to evaluate the *in vitro* skin penetration of CeO_2 by a non-invasive method. The penetration of CeO_2 NPs into the skin was performed in Franz cells with NTO*.

The preparation of skin samples was carried out as described previously, except that the skin samples were not exposed to POX. After leaving the cells for 30 min in a water bath at 37°C, 36 mg of CeO_2 were deposited onto the skin. After 24 h, the donor compartment of the Franz cell was removed and the skin surface was carefully blotted with absorbent paper. This step allows the removal of most of the NPs that could disturb the visualization of skin keratinocytes in Raman experiment. At the end of the experiment, the receptor compartment was connected to an infusion bag in order to keep the skin hydrated during Raman acquisition. The presence of the NPs in the *stratum corneum* layer was performed using confocal Raman microspectroscopy (MCR) (LabRAM HR®, Horiba scientific) and a confocal microscope probe (BXFM Olympus). The objective used in this experiment had a long working distance of magnitude 100x. The excitation source was a red 785 nm laser. The acquisition time was about 30 s and covered the signals corresponding to the skin (including a characteristic peak at 1000 cm^{-1}) and the peak corresponding to ceria (463 cm^{-1}). Spectra were recorded from the surface (Z = -2 µm) up to 30 µm under the surface. The baseline was corrected using an automatic polynomial function. For each depth Z, 3 or 5 spectra were acquired. For each skin sample, the profile of CeO_2 penetration was performed on three different points on the skin surface. For data analysis, the ratio I_{463}/I_{1000} (ratio intensity of the peak at 463 cm^{-1}/ intensity of the peak at 1000 cm^{-1}) was determined as it reflects the presence of ceria in the skin. The means of the ratio for each Z is indicated with its standard error of the mean (SEM., n = 3).

ASSOCIATED CONTENT

DATA AVAILABILITY STATEMENT

The data supporting the findings of this study are available within the main text of this article and its Supporting Information. Further information about this study is available from the corresponding authors upon reasonable request.

SUPPORTING INFORMATION

Refined lattice parameter a, and relative intensity ratio I_D/I_{F2g} of the different morphologies.

XPS spectrum collected for NPO/NTO* and NR/NR*

Degradation kinetics of POX depending on the pH with or without NPs.

CeO_2 nanoparticles skin penetration study by Confocal Raman microspectroscopy.

AUTHOR INFORMATION

CORRESPONDING AUTHORS

Eloise Thomas, Universite Claude Bernard Lyon 1, LAGEPP UMR5007 CNRS, 43 boulevard du 11 novembre 1918, Bâtiment CPE, 69622, Villeurbanne Cedex, France. eloise.thomas@univ-lyon1.fr

Marie-Alexandrine Bolzinger, Universite Claude Bernard Lyon 1, LAGEPP UMR5007 CNRS, 43 boulevard du 11 novembre 1918, Bâtiment CPE, 69622, Villeurbanne Cedex, France. marie.bolzinger@univ-lyon1.fr

AUTHOR CONTRIBUTIONS

The manuscript was written through contributions of all authors. All authors have given approval to the final version of the manuscript. ET supervised part of project (degradation kinetic experiments and in vitro experiments on Franz cells), performed related experiments and analysis, and wrote the article. SB obtained the funding supporting this project, conceived the presented idea and supervised the findings of this work, provided resources to perform the experiments, contributed to the manuscript. GCM, IT, DA and CB performed some of the experiments presented in this article. DA, TD, FC synthesized and characterized the nanoparticles. IP developed the degradation kinetic model. KMV and MB characterized the nanoparticles by microscopy. MAB conceived the presented idea and supervised the findings of this work, obtained the funding supporting this project, provided resources to perform the experiments, contributed to the manuscript.

NOTES

The authors declare that they have no competing financial interests or personal relationships that could have appeared to influence the work reported in this paper.

ACKNOWLEDGMENTS

Luiz Cardenas from IRCELYON (France) is greatly acknowledged for the XPS experiments. The authors are thankful to Tiffanie Salas for drawing the Figure 5. This work was supported by the Direction Générale de l'Armement (DGA – French Procurement agency, PhD grant) and from the DGA ASTRID program (project NanoDeTox – Grant no. ANR-16-ASTR-0008). We thank the Coslife platform for the equipment used in the project.

REFERENCES

(1) Ederer, J.; Janoš, P.; Šťastný, M.; Henych, J.; Ederer, K.; Slušná, M. Š.; Tolasz, J. Nanocrystalline Cerium Oxide for Catalytic Degradation of Paraoxon Methyl: Influence of CeO2 Surface Properties. *J. Environ. Chem. Eng.* **2021**, *9* (5), 106229. https://doi.org/10.1016/j.jece.2021.106229.

(2) Forest, V.; Leclerc, L.; Hochepied, J.-F.; Trouvé, A.; Sarry, G.; Pourchez, J. Impact of Cerium Oxide Nanoparticles Shape on Their in Vitro Cellular Toxicity. *Toxicol. in Vitro* **2017**, *38*, 136–141. https://doi.org/10.1016/j.tiv.2016.09.022.

(3) Salerno, A.; Devers, T.; Bolzinger, M.-A.; Pelletier, J.; Josse, D.; Briançon, S. In Vitro Skin Decontamination of the Organophosphorus Pesticide Paraoxon with Nanometric Cerium Oxide CeO 2. *Chem.-Biol. Interact.* **2017**, *267*, 57–66. https://doi.org/10.1016/j.cbi.2016.04.035.

(4) Salerno, A.; Pitault, I.; Devers, T.; Pelletier, J.; Briançon, S. Model-Based Optimization of Parameters for Degradation Reaction of an Organophosphorus Pesticide, Paraoxon, Using CeO2 Nanoparticles in Water Media. *Environ.Toxicol. Pharmacol.***2017**, *53*, 18–28. https://doi.org/10.1016/j.etap.2017.04.020.

(5) Vernekar, A. A.; Das, T.; Mugesh, G. Vacancy-Engineered Nanoceria: Enzyme Mimetic Hotspots for the Degradation of Nerve Agents. *Angew. Chem. Int. Ed.* **2016**, *55* (4), 1412–1416. https://doi.org/10.1002/anie.201510355.

(6) Chauhan, S.; Chauhan, S.; D'Cruz, R.; Faruqi, S.; Singh, K. K.; Varma, S.; Singh, M.; Karthik, V. Chemical Warfare Agents. *Environ. Toxicol. Pharmacol.* **2008**, *26* (2), 113–122. https://doi.org/10.1016/j.etap.2008.03.003.

(7) Picard, B.; Chataigner, I.; Maddaluno, J.; Legros, J. Introduction to Chemical Warfare Agents, Relevant Simulants and Modern Neutralisation Methods. *Org. Biomol. Chem.* **2019**, *17* (27), 6528–6537. https://doi.org/10.1039/C9OB00802K.

(8) Magnano, G. C.; Rui, F.; Larese Filon, F. Skin Decontamination Procedures against Potential Hazards Substances Exposure. *Chem.-Biol. Interact.* **2021**, *344*, 109481. https://doi.org/10.1016/j.cbi.2021.109481.

(9) Chan, H. P.; Zhai, H.; Hui, X.; Maibach, H. I. Skin Decontamination: Principles and Perspectives. *Toxicol. Ind. Health* **2013**, *29* (10), 955–968. https://doi.org/10.1177/0748233712448112.

(10) Kashetsky, N.; Law, R. M.; Maibach, H. I. Efficacy of Water Skin Decontamination in Vivo in Humans: A Systematic Review. *J. Appl.Toxicol.* **2022**, *42* (3), 346–359. https://doi.org/10.1002/jat.4230.

(11) Thors, L.; Wigenstam, E.; Qvarnström, J.; Hägglund, L.; Bucht, A. Improved Skin Decontamination Efficacy for the Nerve Agent VX. *Chem.-Biol. Interact.* **2020**, *325*, 109135. https://doi.org/10.1016/j.cbi.2020.109135.

(12) Thors, L.; Koch, M.; Wigenstam, E.; Koch, B.; Hägglund, L.; Bucht, A. Comparison of Skin Decontamination Efficacy of Commercial Decontamination Products Following Exposure to VX on Human Skin. *Chem.-Biol. Interact.* **2017**, *273*, 82–89. https://doi.org/10.1016/j.cbi.2017.06.002.

(13) Matar, H.; Price, S. C.; Chilcott, R. P. Further Studies of the Efficacy of Military, Commercial and Novel Skin Decontaminants against the Chemical Warfare Agents Sulphur Mustard, Soman and VX. *Toxicol. in Vitro* **2019**, *54*, 263–268. https://doi.org/10.1016/j.tiv.2018.10.008.

(14) Matar, H.; Guerreiro, A.; Piletsky, S. A.; Price, S. C.; Chilcott, R. P. Preliminary Evaluation of Military, Commercial and Novel Skin Decontamination Products against a

Chemical Warfare Agent Simulant (Methyl Salicylate). *Cutan. Ocul. Toxicol.* **2016**, *35* (2), 137–144. https://doi.org/10.3109/15569527.2015.1072544.
(15) Rolland, P.; Bolzinger, M.-A.; Cruz, C.; Josse, D.; Briançon, S. Hairy Skin Exposure to VX in Vitro: Effectiveness of Delayed Decontamination. *Toxicol. in Vitro* **2013**, *27* (1), 358–366. https://doi.org/10.1016/j.tiv.2012.08.014.
(16) Cao, Y.; Hui, X.; Zhu, H.; Elmahdy, A.; Maibach, H. In Vitro Human Skin Permeation and Decontamination of 2-Chloroethyl Ethyl Sulfide (CEES) Using Dermal Decontamination Gel (DDGel) and Reactive Skin Decontamination Lotion (RSDL). *Toxicol. Lett.* **2018**, *291*, 86–91. https://doi.org/10.1016/j.toxlet.2018.04.015.
(17) Braue, E. H.; Smith, K. H.; Doxzon, B. F.; Lumpkin, H. L.; Clarkson, E. D. Efficacy Studies of Reactive Skin Decontamination Lotion, M291 Skin Decontamination Kit, 0.5% Bleach, 1% Soapy Water, and Skin Exposure Reduction Paste Against Chemical Warfare Agents, Part 2: Guinea Pigs Challenged with Soman. *Cutan. Ocul. Toxicol.* **2011**, *30* (1), 29–37. https://doi.org/10.3109/15569527.2010.515281.
(18) Feschuk, A. M.; Law, R. M.; Maibach, H. I. A Review of Reactive Skin Decontamination Lotion Efficacy. In *Dermal Absorption and Decontamination: A Comprehensive Guide*; Feschuk, A. M., Law, R. M., Maibach, H. I., Eds.; Springer International Publishing: Cham, 2022; pp 133–145. https://doi.org/10.1007/978-3-031-09222-0_8.
(19) Feschuk, A. M.; Law, R. M.; Maibach, H. I. Comparative Efficacy of Reactive Skin Decontamination Lotion (RSDL): A Systematic Review. *Toxicol. Lett.* **2021**, *349*, 109–114. https://doi.org/10.1016/j.toxlet.2021.06.010.
(20) D. Schwartz, M.; G. Hurst, C.; A. Kirk, M.; J.D. Reedy, S.; H. Braue, E. Reactive Skin Decontamination Lotion (RSDL) for the Decontamination of Chemical Warfare Agent (CWA) Dermal Exposure. *Cur. Pharm. Biotechnol.***2012**, *13* (10), 1971–1979. https://doi.org/10.2174/138920112802273191.
(21) Trenque, I.; Camilla Magnano, G.; Bárta, J.; Chaput, F.; Alexandrine Bolzinger, M.; Pitault, I.; Briançon, S.; Masenelli-Varlot, K.; Bugnet, M.; Dujardin, C.; Čuba, V.; Amans, D. Synthesis Routes of CeO 2 Nanoparticles Dedicated to Organophosphorus Degradation: A Benchmark. *CrystEngComm* **2020**, *22* (10), 1725–1737. https://doi.org/10.1039/C9CE01898K.
(22) Trenque, I.; Magnano, G. C.; Bolzinger, M. A.; Roiban, L.; Chaput, F.; Pitault, I.; Briançon, S.; Devers, T.; Masenelli-Varlot, K.; Bugnet, M.; Amans, D. Shape-Selective Synthesis of Nanoceria for Degradation of Paraoxon as a Chemical Warfare Simulant. *Phys. Chem. Chem. Phys.* **2019**, *21* (10), 5455–5465. https://doi.org/10.1039/C9CP00179D.
(23) Thomas, E.; Bordes, C.; Chaput, F.; Arquier, D.; Briançon, S.; Bolzinger, M.-A. CeO2-Based Peelable Gel for Neutralization and Skin Decontamination toward Chemical Warfare Agents. *Colloids Surf. A: Physicochem. Eng. Asp.* **2024**, 133520. https://doi.org/10.1016/j.colsurfa.2024.133520.
(24) Tolasz, J.; Henych, J.; Šťastný, M.; Němečková, Z.; Šrámová Slušná, M.; Opletal, T.; Janoš, P. Room-Temperature Synthesis of Nanoceria for Degradation of Organophosphate Pesticides and Its Regeneration and Reuse. *RSC Adv.* **2020**, *10* (24), 14441–14450. https://doi.org/10.1039/D0RA00937G.
(25) Janoš, P.; Henych, J.; Pelant, O.; Pilařová, V.; Vrtoch, L.; Kormunda, M.; Mazanec, K.; Štengl, V. Cerium Oxide for the Destruction of Chemical Warfare Agents: A Comparison of Synthetic Routes. *J. Hazard. Mater.* **2016**, *304*, 259–268. https://doi.org/10.1016/j.jhazmat.2015.10.069.

(26) Janoš, P.; Ederer, J.; Došek, M.; Štojdl, J.; Henych, J.; Tolasz, J.; Kormunda, M.; Mazanec, K. Can Cerium Oxide Serve as a Phosphodiesterase-Mimetic Nanozyme? *Environ. Sci.: Nano* **2019**, *6* (12), 3684–3698. https://doi.org/10.1039/C9EN00815B.
(27) Ederer, J.; Novák, A.; Janoš, P.; Šťastný, M.; Henych, J.; Bárta, M.; Ryšánek, P.; Tolasz, J. Influence of Surface Chemical Properties of Nanocrystalline CeO2 on Phosphate Adsorption and Methyl-Paraoxon Decomposition. *J. Ind. Eng. Chem.* **2023**, *123*, 125–139. https://doi.org/10.1016/j.jiec.2023.03.029.
(28) Henych, J.; Šťastný, M.; Ederer, J.; Němečková, Z.; Pogorzelska, A.; Tolasz, J.; Kormunda, M.; Ryšánek, P.; Bażanów, B.; Stygar, D.; Mazanec, K.; Janoš, P. How the Surface Chemical Properties of Nanoceria Are Related to Its Enzyme-like, Antiviral and Degradation Activity. *Environ. Sci.: Nano* **2022**, *9* (9), 3485–3501. https://doi.org/10.1039/D2EN00173J.
(29) Zhan, S.-W.; Tseng, W.-B.; Tseng, W.-L. Impact of Nanoceria Shape on Degradation of Diethyl Paraoxon: Synthesis, Catalytic Mechanism, and Water Remediation Application. *Environ. Res.* **2020**, *188*, 109653. https://doi.org/10.1016/j.envres.2020.109653.
(30) Goris, B.; Turner, S.; Bals, S.; Van Tendeloo, G. Three-Dimensional Valency Mapping in Ceria Nanocrystals. *ACS Nano* **2014**, *8* (10), 10878–10884. https://doi.org/10.1021/nn5047053.
(31) Miri, P.; Karbhal, I.; Satnami, M. L.; Jena, V. K.; Ghosh, S. β-Cyclodextrin Stabilized Nanoceria for Hydrolytic Cleavage of Paraoxon in Aqueous and Cationic Micellar Media. *ACS Appl. Bio Mater.* **2023**, *6* (4), 1488–1494. https://doi.org/10.1021/acsabm.2c01030.
(32) Kuchma, M. H.; Komanski, C. B.; Colon, J.; Teblum, A.; Masunov, A. E.; Alvarado, B.; Babu, S.; Seal, S.; Summy, J.; Baker, C. H. Phosphate Ester Hydrolysis of Biologically Relevant Molecules by Cerium Oxide Nanoparticles. *Nanomedicine: NBM* **2010**, *6* (6), 738–744. https://doi.org/10.1016/j.nano.2010.05.004.
(33) Vallet, V.; Cruz, C.; Licausi, J.; Bazire, A.; Lallement, G.; Boudry, I. Percutaneous Penetration and Distribution of VX Using in Vitro Pig or Human Excised Skin: Validation of Demeton-S-Methyl as Adequate Simulant for VX Skin Permeation Investigations. *Toxicology* **2008**, *246* (1), 73–82. https://doi.org/10.1016/j.tox.2007.12.027.
(34) Lademann, J.; Patzelt, A.; Schanzer, S.; Richter, H.; Gross, I.; Menting, K. H.; Frazier, L.; Sterry, W.; Antoniou, C. Decontamination of the Skin with Absorbing Materials. *Skin Pharmacol. Physiol.* **2010**, *24* (2), 87–92. https://doi.org/10.1159/000322305.
(35) Wilson, C.; Cooper, N. J.; Briggs, M. E.; Cooper, A. I.; Adams, D. J. Investigating the Breakdown of the Nerve Agent Simulant Methyl Paraoxon and Chemical Warfare Agents GB and VX Using Nitrogen Containing Bases. *Org. Biomol. Chem.* **2018**, *16* (47), 9285–9291. https://doi.org/10.1039/C8OB02475H.
(36) Pavez, P.; Millán, D.; Morales, J. I.; Castro, E. A.; López A., C.; Santos, J. G. Mechanisms of Degradation of Paraoxon in Different Ionic Liquids. *J. Org. Chem.* **2013**, *78* (19), 9670–9676. https://doi.org/10.1021/jo401351v.
(37) Kumar, J. P.; Ramacharyulu, P. V. R. K.; Prasad, G. K.; Srivastava, A. R.; Singh, B. Molecular Sieves Supported with Metal Oxide Nanoparticles: Synthesis, Characterization and Decontamination of Sulfur Mustard. *J. Porous Mat.* **2015**, *22* (1), 91–100. https://doi.org/10.1007/s10934-014-9876-6.
(38) Bisio, C.; Carniato, F.; Palumbo, C.; Safronyuk, S. L.; Starodub, M. F.; Katsev, A. M.; Marchese, L.; Guidotti, M. Nanosized Inorganic Metal Oxides as Heterogeneous Catalysts for the Degradation of Chemical Warfare Agents. *Catal. Today* **2016**, *277*, 192–199. https://doi.org/10.1016/j.cattod.2015.12.023.

(39) Prasad, G. K.; Ramacharyulu, P. V. R. K.; Batra, K.; Singh, B.; Srivastava, A. R.; Ganesan, K.; Vijayaraghavan, R. Decontamination of Yperite Using Mesoporous Mixed Metal Oxide Nanocrystals. *J. Hazard. Mater.* **2010**, *183* (1), 847–852. https://doi.org/10.1016/j.jhazmat.2010.07.104.
(40) Kiani, A.; Dastafkan, K. Zinc Oxide Nanocubes as a Destructive Nanoadsorbent for the Neutralization Chemistry of 2-Chloroethyl Phenyl Sulfide: A Sulfur Mustard Simulant. *J. Colloid Interf. Science* **2016**, *478*, 271–279. https://doi.org/10.1016/j.jcis.2016.06.025.
(41) Kim, K.; Tsay, O. G.; Atwood, D. A.; Churchill, D. G. Destruction and Detection of Chemical Warfare Agents. *Chem. Rev.* **2011**, *111* (9), 5345–5403. https://doi.org/10.1021/cr100193y.
(42) Sellik, A.; Pollet, T.; Ouvry, L.; Briancon, S.; Fessi, H.; Hartmann, D. J.; Renaud, F. N. R. Degradation of Paraoxon (VX Chemical Agent Simulant) and Bacteria by Magnesium Oxide Depends on the Crystalline Structure of Magnesium Oxide. *Chem.-Biol. Interact.* **2017**, *267*, 67–73. https://doi.org/10.1016/j.cbi.2016.11.023.
(43) Janos, P.; Kuran, P.; Kormunda, M.; Stengl, V.; Grygar, T. M.; Dosek, M.; Stastny, M.; Ederer, J.; Pilarova, V.; Vrtoch, L. Cerium Dioxide as a New Reactive Sorbent for Fast Degradation of Parathion Methyl and Some Other Organophosphates. *J. Rare Earths* **2014**, *32* (4), 360–370. https://doi.org/10.1016/S1002-0721(14)60079-X.
(44) Li, T.; Tsyshevsky, R.; Algrim, L.; McEntee, M.; Durke, E. M.; Eichhorn, B.; Karwacki, C.; Zachariah, M. R.; Kuklja, M. M.; Rodriguez, E. E. Understanding Dimethyl Methylphosphonate Adsorption and Decomposition on Mesoporous CeO $_2$. *ACS Appl. Mater. Interf.* **2021**, *13* (45), 54597–54609. https://doi.org/10.1021/acsami.1c16668.
(45) Kumar, J. P.; P.V.R.K., R.; G.K., P.; Singh, B. Montmorillonites Supported with Metal Oxide Nanoparticles for Decontamination of Sulfur Mustard. *Appl. Clay Sci.* **2015**, *116–117*, 263–272. https://doi.org/10.1016/j.clay.2015.04.007.
(46) Maksimović, Ž. M.; Škrbić, R.; Stojiljković, M. P. Dose-Dependency of Toxic Signs and Outcomes of Paraoxon Poisoning in Rats. *Acta Med.* **2022**, *65* (1), 8–17. https://doi.org/10.14712/18059694.2022.10.
(47) Eichenbaum, G.; Johnson, M.; Kirkland, D.; O'Neill, P.; Stellar, S.; Bielawne, J.; DeWire, R.; Areia, D.; Bryant, S.; Weiner, S.; Desai-Krieger, D.; Guzzie-Peck, P.; Evans, D. C.; Tonelli, A. Assessment of the Genotoxic and Carcinogenic Risks of P-Nitrophenol When It Is Present as an Impurity in a Drug Product. *Reg. Toxicol. Pharmacol.* **2009**, *55* (1), 33–42. https://doi.org/10.1016/j.yrtph.2009.05.018.
(48) V. Plakhova, T.; Yu. Romanchuk, A.; M. Butorin, S.; D. Konyukhova, A.; V. Egorov, A.; A. Shiryaev, A.; E. Baranchikov, A.; V. Dorovatovskii, P.; Huthwelker, T.; Gerber, E.; Bauters, S.; M. Sozarukova, M.; C. Scheinost, A.; K. Ivanov, V.; N. Kalmykov, S.; O. Kvashnina, K. Towards the Surface Hydroxyl Species in CeO 2 Nanoparticles. *Nanoscale* **2019**, *11* (39), 18142–18149. https://doi.org/10.1039/C9NR06032D.
(49) Wu, Z.; Li, M.; Overbury, S. H. On the Structure Dependence of CO Oxidation over CeO2 Nanocrystals with Well-Defined Surface Planes. *J. Catal.* **2012**, *285* (1), 61–73. https://doi.org/10.1016/j.jcat.2011.09.011.
(50) Mann, A. K. P.; Wu, Z.; Calaza, F. C.; Overbury, S. H. Adsorption and Reaction of Acetaldehyde on Shape-Controlled CeO2 Nanocrystals: Elucidation of Structure–Function Relationships. *ACS Catal.* **2014**, *4* (8), 2437–2448. https://doi.org/10.1021/cs500611g.
(51) Ederer, J.; Janoš, P.; Vrtoch, L.; Štastný, M.; Henych, J.; Matoušek, J.; Kormunda, M.; Ryšánek, P. Effect of Surface Treatment of Nanocrystalline CeO $_2$ on Its Dephosphorylation Activity and Adsorption of Inorganic Phosphates. *Langmuir* **2024**, *40* (1), 302–316. https://doi.org/10.1021/acs.langmuir.3c02576.

(52) Vincent, A.; Inerbaev, T. M.; Babu, S.; Karakoti, A. S.; Self, W. T.; Masunov, A. E.; Seal, S. Tuning Hydrated Nanoceria Surfaces: Experimental/Theoretical Investigations of Ion Exchange and Implications in Organic and Inorganic Interactions. *Langmuir* **2010**, *26* (10), 7188–7198. https://doi.org/10.1021/la904285g.
(53) Fentabil, M.; Gebremedhin, M.; Purdon, J. G.; Cochrane, L.; Goldman, V. S. Degradation of Pesticides with RSDL® (Reactive Skin Decontamination Lotion Kit) Lotion: LC–MS Investigation. *Toxicol. Lett.* **2018**, *293*, 241–248. https://doi.org/10.1016/j.toxlet.2017.11.003.
(54) Bogan, R.; Maas, H. J.; Zimmermann, T. Chemical Stability of Reactive Skin Decontamination Lotion (RSDL®). *Toxicol. Lett.* **2018**, *293*, 264–268. https://doi.org/10.1016/j.toxlet.2017.09.016.
(55) Larese Filon, F.; Mauro, M.; Adami, G.; Bovenzi, M.; Crosera, M. Nanoparticles Skin Absorption: New Aspects for a Safety Profile Evaluation. *Reg. Toxicol. Pharmacol.* **2015**, *72* (2), 310–322. https://doi.org/10.1016/j.yrtph.2015.05.005.
(56) Salerno, A.; Bolzinger, M. A.; Rolland, P.; Chevalier, Y.; Josse, D.; Briançon, S. Pickering Emulsions for Skin Decontamination. *Toxicol. in Vitro* **2016**, *34*, 45–54. https://doi.org/10.1016/j.tiv.2016.03.005.